Journal of Computational Chemistry

WILEY

Journal of COMPUTATIONAL CHEMISTRY

RESEARCH ARTICLE OPEN ACCESS

Collective Interactions in Ion Pairs

Jorge Gonzalo[1] | Julen Munárriz[1] | Angel Martín Pendás[2] | Jorge Echeverría[3]

[1]Departamento de Química Física and Instituto de Biocomputación y Física de Sistemas Complejos (BIFI), Universidad de Zaragoza, Zaragoza, Spain | [2]Departamento de Química Física y Analítica, Universidad de Oviedo, Oviedo, Spain | [3]Instituto de Síntesis Química y Catalisis Homogénea (ISQCH) and Departmento de Química Inorgánica, Facultad de Ciencias, Universidad de Zaragoza, Zaragoza, Spain

Correspondence: Jorge Echeverría (jorge.echeverria@unizar.es)

Received: 8 April 2026 | **Revised:** 13 May 2026 | **Accepted:** 15 May 2026

ABSTRACT

Collective interactions represent a recently proposed bonding mode in which stabilization arises not from a localized two-center bond but from the distributed exchange–correlation effects between a central site and several surrounding atoms, whereas the interaction between the central atom and the metal is destabilizing. While this phenomenon has been demonstrated in certain organometallic complexes, its possible existence in predominantly ionic systems remains unexplored. Here, we present a comprehensive study on a family of ion pairs of general formula $M[AX_4]$ ($M = Li^+$, Na^+, K^+, Rb^+, Cs^+; A = B, Fe Co, Zn, Cd; X = $-CH_3$, –CO, –CCH, $-OCH_3$, –Cl) aimed at determining whether collective interactions can arise in systems conventionally described as ionic. Through a combination of penetration index analysis and Interacting Quantum Atoms (IQA) decomposition, we quantify the contributions of Coulombic and exchange–correlation terms to the total interaction energy. The calculated exchange–correlation interaction collectivity indices (ICI_{XC}) reveal that alkali metal–tetramethylborate ion pairs and several transition metal tetrahedral anions exhibit distinctly collective behavior, particularly when complexes possess electron-rich or polarizable ligands (–CCH, $-OCH_3$, –Cl). In contrast, carbonyl-containing systems display larger ICI_{XC} values, consistent with a classical noncollective bonding scheme. These results demonstrate that collective interactions can indeed manifest in ionic environments, extending the scope of the concept beyond covalent or organometallic frameworks and offering new insights into the fundamental nature of ion pairing and electronic delocalization.

1 | Introduction

Chemical bonding has traditionally been categorized into well-established motifs, namely covalent and ionic, dative, charge-shift, and various multicenter bonding frameworks, such as 3c–4e, each reflecting different ways that electrons can be shared or exchanged between atoms. However, emerging research suggests that this classical taxonomy may be overlooking subtler bonding phenomena that lie outside the conventional two-electron, two-center paradigm [1]. One particularly riveting example is the so-called *collective interaction* in organometallic complexes of general formula MAX_3, a recently described bonding mode in which a metal center (M) interacts not solely with a close central atom (A = boron, aluminum, carbon, etc.), but also significantly with the substituents attached to that atom (X) [2]. As a consequence, the weak (destabilizing) interaction of the metal with the central atom (M···A) is compensated by the stabilizing interactions between the former and the adjacent groups (M···X). Since the original publication in 2022 [2], the concept of collective interactions has been the subject of intense debate in the chemical bonding community [3–6].

Recent work on organometallic reagents, such as organolithium and Grignard compounds, highlights that these collective interactions are common in systems once assumed to be primarily based on classical interactions [2]. In these species, the net stabilization arises not so much from a pairwise metal–central-atom bond, but rather from a network of weaker, yet cumulatively significant, interactions between the metal and peripheral groups such as hydrides, alkyl substituents, fluorines, etc. This

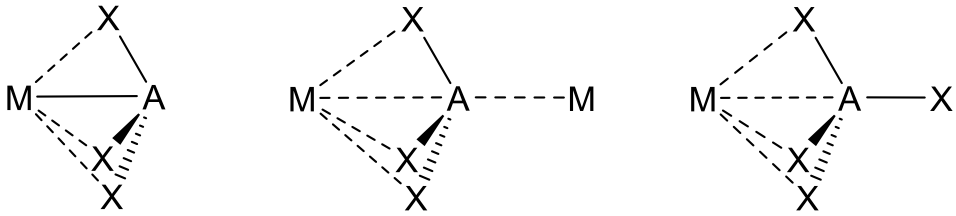

SCHEME 1 | Structural motifs previously known to display collective interactions (MAX_3 and M_2AX_3) and ion pairs studied in this work (MAX_4).

insight challenges the Lewis-based picture in which the metal is depicted as bonded directly to the central atom, while the substituents serve merely as spectators. To quantify the extent of these multifaceted interactions, a new index was introduced: the *exchange-correlation interaction collectivity index* (ICI_{XC}). This index compares the share of exchange-correlation energy from conventional, pairwise interactions against the share distributed over the rest of the molecule. When ICI_{XC} approaches unity, the bonding more closely resembles a traditional two-center bond, whereas when it departs significantly from unity, the bond's character reflects collective, many-atom interactions.

In the context of collective interactions, geometry plays a crucial role in enabling a metal (or other bonding partner) to distribute its stabilizing exchange-correlation effects across multiple nearby substituents, rather than focusing exclusively on a single atom. While there is no single, rigid structural formula that guarantees collective interactions, studies to date point to a few common geometric features that favor this many-atom bonding mode [2]. A key requirement is that the putative collective center (e.g., a metal) be positioned such that it can have meaningful (often short-to-moderate) noncovalent contacts with several peripheral atoms rather than engaging in a single dominant two-center bond. For instance, in organometallics featuring MAX_3 units, the metal is often near the substituents (X) on the central atom (A) at distances where partial exchange-correlation interactions can occur (Scheme 1) [7].

Many examples of collective interactions appear in or near symmetrical geometries (e.g., D_{3h}, C_{3v}, or slightly distorted variants). These symmetries allow the metal center or positively charged site to align effectively with all substituents, ensuring each substituent is close enough to participate in bonding-like interactions. Additionally, such arrangements prevent the system from collapsing into a single, strong two-atom bond at the expense of the others. Furthermore, quantum chemical topology [8] analyzes often reveal more than one bond path or critical point connecting a metal with various substituents in collective-bonding scenarios [9], especially in geometries where the central atom is somewhat displaced and the metal is effectively closer to the substituents than to the central atom. It is worth noting that while having multiple bond paths does not by itself prove collective interactions, it often signals that the metal is engaging in multiple, partial stabilizing contacts.

In some molecules, particularly those featuring heavier metals or strongly electron-withdrawing substituents, the system may adopt an inverted geometry in which the central atom is bent away from the metal, giving the substituents more direct contact with that metal center. These inverted local minima often show the most pronounced collective interactions because the geometry maximizes metal–substituent overlap, even though it departs from what a simple Lewis or ionic model would predict. An example of this behavior is found, for instance, in trigonal bipyramidal alkaline metal-boron halide complexes of general formula M_2AX_3 (A = B; Scheme 1) [9].

As mentioned above, collective interactions arise when a bonding center extends its stabilizing exchange-correlation influence through multiple atoms at once, rather than channeling it solely into a single, two-center bond. In terms of charges and electronic structure, there are some features that seem to facilitate this behavior. First, there must be an electron-deficient center or cationic region, often a metal or positively polarized atom, capable of receiving electron density from multiple directions. This partial or formal positive charge promotes simultaneous attraction to several negatively charged or electron-rich groups. Second, the system requires substituents with partial negative charges or accessible electron density. These substituents, such as hydrides, alkyls, or electronegative ligands, offer alternative sites for bonding interactions, enabling a more "spread-out" form of stabilization than a single localized bond could provide. Third, the molecule needs an electronic structure flexible enough to delocalize or distribute these interactions. This flexibility typically arises from orbitals that allow partial electron sharing with several neighbors. When these conditions converge, the result is a network of multiatom bonding contributions whose cumulative effect significantly stabilizes the system. The traditional two-center model often underestimates this additional stabilization because it focuses primarily on a single bond and relegates other contacts to mere noncovalent interactions.

Based on a recent computational study that suggested a more complex chemical bonding scenario than expected in tetramethylammonium-halide pairs [10], this article aims to investigate whether collective interactions can arise even in nominally ionic pairs of formula MAX_4 (Scheme 1), systems traditionally viewed as governed predominantly by electrostatic attractions. If such interactions exist in different strongly polarized or near-ionic environments, it would call for a reexamination of how we define, classify, and predict the properties of several ionic compounds. By combining computational analyses with theoretical insights into exchange-correlation effects, we seek to determine whether the stabilizing-destabilizing network of interactions documented in certain organometallic species can also appear in simpler ionic pairs and what the requirements

(in terms of geometry, electronic structure, etc.) of the involved ions are to engage in collective interactions. Establishing the presence of collective interactions in common ion pairs will help refine our knowledge of chemical bonding, offering new perspectives on how ions assemble, react, and stabilize in complex chemical environments.

2 | Methods

For the structural analysis of interatomic interactions we use the penetration index [10, 11]. The penetration index for an A–B atom pair (p_{AB}) is defined as $p_{AB} = 100 \cdot (v_A + v_B - d_{AB})/(v_A + v_B - r_A - r_B)$, where d is the interatomic distance between atoms A and B, and r and v are the corresponding covalent [12] and van der Waals radii [13], respectively. When two atoms lie at a separation equal to their summed van der Waals radii, the penetration index p_{AB} is 0%. As they move closer to a distance defined by the sum of their covalent radii, p_{AB} rises to 100%. For separations in between these two extremes, p_{AB} adopts intermediate values, reflecting weaker or noncovalent forms of interaction. Moreover, p_{AB} can adopt values over 100% for distances shorter than the sum of the covalent radii and under 0% for distances longer than the sum of the van de Waals radii. The use of this parameter offers several advantages over relying on simple interatomic distances because it provides a size-corrected, unified measure of how deeply two atoms' outer regions overlap regardless of the nature of the atoms [14, 15]. Despite based on covalent radii, penetration indices have been successfully used for the analysis of ionic solids since the sum of cationic and anionic radii for atoms A and B yields a value that is very close to the sum of the corresponding covalent radii [11].

The energetics of the ion-pair interactions, as well as the assessment of whether these interactions are collective in nature, were examined using the Interacting Quantum Atoms (IQA) energy-decomposition scheme. IQA provides a rigorous partitioning of chemical space based on the topology of a scalar field—here, the electron density. In broad terms, it enables the calculation of interaction energies between predefined fragments (individual atoms or groups of atoms) and decomposes them into two components: an exchange–correlation term (V_{xc}), associated with electron-sharing and regarded as the covalent contribution to bonding, and a classical term (V_{cl}), which reflects the electrostatic component of the interaction [16]. Beyond its role in establishing the concept of collective interactions, this framework has been broadly employed to characterize chemical bonding in exotic regimes and in metal-based systems [17–20], among other applications that have been reviewed elsewhere [21]. The V_{XC} term provided by IQA decomposition also allows us to determine whether a given chemical interaction is collective or not. Namely, the exchange-correlation interaction collectivity index (ICI_{XC}) for atom M in MAX_n systems (Scheme 1) is defined as the ratio between V_{XC}(M,A) and V_{XC}(M,T), where T stands for all atoms in the system except M [2]. ICI_{XC} is equal to 1 in diatomic species and diminishes as the number of atoms in the molecule increases, approaching zero for systems displaying collective interactions.

Geometry optimizations and energy calculations of coordination complexes were conducted with the B3LYP exchange correlation functional, in conjunction with the D3BJ empirical dispersion correction scheme; while tetramethylborate-based species were calculated with the M06-2X functional. In all cases, we considered the Ahlrichs def2-TZVPP basis sets, as implemented in the Gaussian16 software package [22]. To obtain all-electron wavefunctions for the IQA analysis, we performed single-point energy calculations using ORCA 5.0 package [23]. For systems including Rb or Cs atoms, we applied the zeroth-order regular approximation (ZORA) to account for relativistic effects. In these calculations, we employed the SARC/J auxiliary basis sets and the SARC-ZORA-TZVPP basis set for Rb and Cs. To accelerate the calculations, the RIJCOSX approximation was applied.

IQA and QTAIM calculations were performed on the single-determinant all-electron M06-2X and B3LYP pseudo-wavefunctions by means of the AIMALL package [24], using the program's default integration algorithms.

3 | Results and Discussion

In light of the aforementioned electronic and geometric motifs, a promising way to broaden the scope of collective interactions in ionic systems is to look at tetrahedral or near-tetrahedral architectures. We have chosen tetramethylborate $[B(CH_3)_4]^-$ (TMB) as the tetrahedral anionic system. Then, a monoatomic cation can be placed near one of the tetrahedral faces of TMB (κ^3 interaction), mirroring geometries known to favor collective interactions (Scheme 2). Although these salts might initially appear governed mostly by ionic attractions, their structural similarity to previously studied organometallics suggests that they, too, may exhibit many-atom interactions. Consequently, if such collective effects are indeed operative in these seemingly straightforward ionic complexes, then part of their overall stability would arise not merely from electrostatic attractions but from distributed exchange-correlation contributions as well.

In order to test our hypothesis, we have optimized the geometries of ion pairs of general formula MAX_4, where $A = B^-$, $M = Li^+$, Na^+, K^+, Rb^+, Cs^+ and $X = CH_3$ (i.e., alkali metal-TMB pairs). In these systems, the monoatomic cation M can interact with a tetrahedral moiety of TMB in a κ^3 fashion, as depicted in Scheme 2. Relevant penetration indices of the optimized

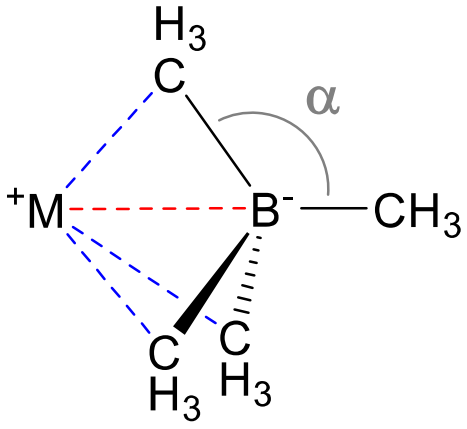

SCHEME 2 | Interaction of M^+ with $[B(CH_3)_4]^-$ involving three methyl groups in a κ^3 fashion.

structures are shown in Table 1. It is worth mentioning that $[B(CH_3)_4]^-Cs^+$ could not be obtained in a κ^3 fashion since geometry optimizations ended up in κ^2 interaction topology with two shorter Cs···C distances. If we look at the penetration indices, it can be observed that they are higher for the B–M pairs, with p_{MB} values typical of covalent bonds (99.7%–108.4%), while they are lower for M–C and M–H atomic pairs. This indicates that the interaction of the alkali metal cation with the boron center is not negligible and can determine the nature of the bonding in these systems.

The main IQA parameters for the alkali metal–TMB pairs are summarized in Table 2. Both the metal (M) and boron (A) atoms exhibit positive atomic charges, which indicates the presence of a Coulombic repulsion between these two atoms. This is confirmed by the positive values of V_C(M,A), reflecting an overall repulsive interaction in all analyzed systems (E_{int}(M,A) > 187 kcal mol^{-1}). In contrast, the exchange–correlation contribution between M and A is minimal, with $|V_{XC}(M,A)| < 3$ kcal mol^{-1}, suggesting a negligible covalent character in this interaction. The principal stabilization within these complexes thus arises from the interaction between the metal and the remainder of the TMB framework, as evidenced by the significantly larger V_{XC}(M,T) values, ranging from −36.9 to −50.1 kcal mol^{-1}. Remarkably, the calculation of the exchange-correlation interaction collectivity indices (ICI_{XC}), with very small values between 0.030 and 0.073 (Table 3), confirms that the interaction of alkali metal cations with TMB is of collective nature.

Next, we broaden our focus to include transition metal anions. We have selected a set of tetrahedral complexes, shown in Scheme 3, containing different ligands (–CO, –CCH, $-OCH_3$, $-CH_3$, and –Cl) and metal centers (Fe, Co, Zn, Cd). We have optimized the geometry of each anionic complex interacting with the five alkali metal cations, and the most relevant penetration indices and α angles are presented in Table 4 (Cartesian coordinates for all optimized complexes are given in Table S1).

All M–A penetration indices exceed 100%, with the highest value observed for ($[Zn(CH_3)_4]Cs$), reaching 125.4%. In most complexes, p_{MA} is greater than p_{MX}, indicating stronger penetration between M and A than between M and X. An exception occurs for the $[ZnCl_4]M$ series (M = K, Rb, Cs), where the M–Cl penetrations slightly surpass the corresponding M–Zn values. Overall, the penetration indices increase systematically down the alkali metal group, reflecting the enhanced overlap associated with the larger cationic radii. It is also worth noting that for carbonyl complexes, metal–ligand associated penetrations (p_{MC} and p_{MO}) are somewhat smaller than those found for other systems with different ligands.

The QTAIM parameters for all ion pairs in Scheme 3 are summarized in Table 5. If we focus first on the atomic charges, some interesting comments can be made. The charge of the alkali metal atom (M) is consistently positive, as expected for a monoatomic cation. In most complexes, the charge exceeds +0.8, except for the Fe-containing tetracarbonylferrates of Na, K, and Rb, where slightly lower values are observed. A general trend is evident across the periodic group: the charge on M becomes progressively less positive as one descends from Li to Cs, reflecting the increasing metallic character and reduced charge localization in larger alkali cations. Notably, this trend is not followed by the Fe and Co carbonyl complexes, which show a relatively constant charge on M, likely due to the distinct electronic environments imposed by the transition metal centers. The atomic charge of the central atom A is also always

TABLE 1 | Relevant penetration indices (%) and average α angle for $M[B(CH_3)_4]$ (M = Li^+, Na^+, K^+, Rb^+, Cs^+) ion pairs.

Ion pair	p_{MB}	P_{MC}	P_{MH}	α (°)
$[B(CH_3)_4]^-Li^+$	108.4	95.5	84.2	108.9
$[B(CH_3)_4]^-Na^+$	105.8	95.7	91.9	106.3
$[B(CH_3)_4]^-K^+$	102.7	94.4	97.4	104.9
$[B(CH_3)_4]^-Rb^+$	99.7	94.3	99.5	104.5
$[B(CH_3)_4]^-Cs^+$	103.9	91.6–107.8	97.6–98.6	—

TABLE 3 | Coulombic (ICI_C) and exchange-correlation (ICI_{XC}) interaction collectivity index values for $M[B(CH_3)_4]$ (M = Li^+, Na^+, K^+, Rb^+, Cs^+) ion pairs calculated at the M06-2X/def2-TZVPP level of theory.

Ion pair	ICI_C	ICI_{XC}
$[B(CH_3)_4]^-Li^+$	−1.851	0.073
$[B(CH_3)_4]^-Na^+$	−1.940	0.054
$[B(CH_3)_4]^-K^+$	−1.997	0.043
$[B(CH_3)_4]^-Rb^+$	−2.002	0.037
$[B(CH_3)_4]^-Cs^+$	−1.978	0.030

TABLE 2 | Relevant atomic charges and IQA parameters for $M[B(CH_3)_4]$ (M = Li^+, Na^+, K^+, Rb^+, Cs^+) ion pairs calculated at the M06-2X/def2-TZVPP level of theory. All energies are given in kcal mol^{-1}.

Ion pair	q(M)	$q(A)_B$	$q(X)_C$	$q(X)_H$	V_{XC}(M,A)	V_{XC}(M,T)	V_C(M,A)	V_C(M,T)	E_{int}(M,A)	E_{int}(M,T)
$[B(CH_3)_4]^-Li^+$	0.891	1.818	−0.476	−0.164	−2.7	−36.9	270.4	−146.0	267.7	−182.9
$[B(CH_3)_4]^-Na^+$	0.904	1.833	−0.447	−0.177	−2.1	−38.8	228.0	−117.5	225.9	−156.3
$[B(CH_3)_4]^-K^+$	0.906	1.834	−0.431	−0.175	−2.0	−45.3	199.6	−99.9	197.6	−145.2
$[B(CH_3)_4]^-Rb^+$	0.905	1.844	−0.438	−0.172	−1.7	−45.8	189.4	−94.6	187.7	−140.4
$[B(CH_3)_4]^-Cs^+$	0.917	1.841	−0.442	−0.137	−1.5	−50.1	189.2	−95.7	187.6	−145.8

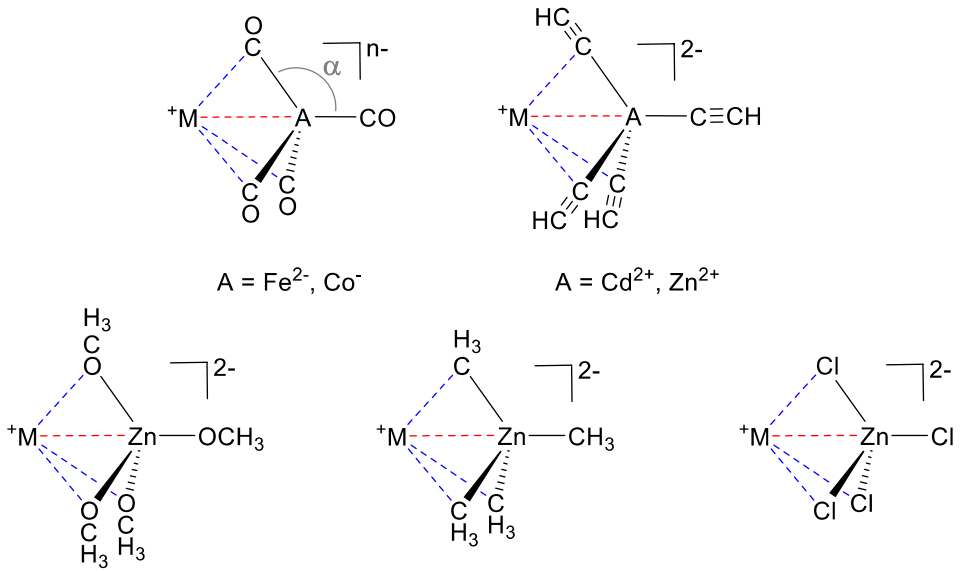

SCHEME 3 | Ion pairs involving transition metal complexes studied in this work.

positive, although its magnitude depends on the metal nature. For Zn and Cd complexes, the charge remains close to +1.0, consistent with their typical divalent character. In contrast, Fe and Co complexes exhibit smaller positive charges, around +0.5, indicating a higher degree of electron sharing with the surrounding carbonyl ligands.

The atomic charges of the ligand atoms display a wide variation depending on the chemical nature of the substituent, reflecting the distinct electronic environments within each functional group. In carbonyl ligands (–CO), the carbon atom bears an average positive charge of +0.76, while the oxygen atom is significantly negative (−1.25), consistent with the strong polarization of the C=O bond and the oxygen's high electronegativity. For the acetylide ligand (–CCH), both carbon atoms are negatively charged (−0.28 for C^1 and −0.52 for C^2), indicating electron density delocalization along the C≡C bond. In the methyl group (–CH_3), the carbon atom carries a modest negative charge (−0.36), while the hydrogen atoms exhibit slightly negative charges (−0.16). The methoxy ligand (–OCH_3) shows a strongly negative oxygen (−1.21) and a positively charged carbon (+0.64), revealing substantial charge separation due to the electron-withdrawing character of oxygen. Finally, in the chloro ligand (–Cl), the chlorine atom possesses a negative charge (−0.78), consistent with its high electronegativity and its role as an electron donor toward the metal center.

We can analyze next the IQA results. The interaction energy components between the alkali metal (M) and the central atom (A) reveal distinct trends across the series. The exchange–correlation term (V_{XC}(M,A)) is very small for the Zn and Cd compounds, indicating negligible covalent character in these interactions, but it becomes noticeably larger for the Fe and Co analogs, suggesting a greater degree of electronic delocalization. In contrast, the classical Coulombic component (V_C(M,A)) is highly repulsive for Zn and Cd complexes and significantly less so for Co and Fe. The strongest repulsion is observed for $[Zn(OCH_3)_4]^{2-}$, with V_C(M,A) values ranging from 137.4 to 178.2 kcal mol^{-1}, consistent with the particularly high positive charge of the Zn center. As a result, the total interaction energy (E_{int}(M,A)) is only slightly repulsive for Fe and Co complexes (10.9–34.6 kcal·mol^{-1}), but strongly repulsive for Zn and Cd (76.9–177.0 kcal mol^{-1}). In contrast, the exchange–correlation term between the alkali metal and the whole molecule, V_{XC}(M,T), remains relatively constant across all systems, while the Coulombic component V_C(M,T) is attractive in every case. However, its magnitude is smaller for $[Co(CO)_4]^-$, likely due to the single negative charge of this complex, which reduces the electrostatic attraction toward the alkali metal cations.

In order to determine whether these ion pairs are held together by collective interactions, we have calculated the corresponding exchange-correlation interaction collectivity indices (ICI_{XC}) that are shown in Table 6. The ICI_{XC} values reveal notable differences in the degree of electronic collectivity among the studied systems. For the tetracarbonylferrate and cobaltate complexes, ICI_{XC} values range between 0.253 and 0.529, indicating the absence of collective interactions and suggesting that the bonding between the alkali metal and the transition metal fragment remains largely localized. In contrast, the methyl complexes exhibit slightly lower ICI_{XC} values, between 0.103 and 0.134, which point to a moderate degree of electronic collectivity. The smallest ICI_{XC} values, below 0.07, are found for the –CCH, –OCH_3, and –Cl derivatives, signifying the presence of distinctly collective interactions in these systems. These results demonstrate that the nature of the ligand exerts a significant influence on the extent of electron delocalization between the alkali metal and the molecular fragments.

Collective behavior seems to arise only when the ligand's electronic structure promotes delocalized charge distribution and/or negatively charged atoms directly bound to the metal center. Ligands such as –CCH, –OCH_3, and –Cl, which exhibit low ICI_{XC} values (< 0.07), fulfill these conditions. Their negative or highly polar atoms enable electron density to extend over multiple bonds, allowing the alkali metal to interact

TABLE 4 | Relevant penetration indices (%) and average α angle for $M[AX_4]$ ($M = Li^+, Na^+, K^+, Rb^+, Cs^+$; A = Fe, Co, Zn, Cd; X = –CO, –CCH, $–OCH_3$, $–CH_3$, and –Cl) ion pairs.

Ion pair	p_{MA}	p_{MC}	p_{MO}	α (°)
$[Co(CO)_4]^-Li^+$	111.9	70.4	18.5	103.4
$[Co(CO)_4]^-Na^+$	113.6	75.4	26.7	102.4
$[Co(CO)_4]^-K^+$	108.7	80.7	45.6	107.0
$[Co(CO)_4]^-Rb^+$	108.0	86.7	62.3	107.9
$[Co(CO)_4]^-Cs^+$	109.3	90.5	72.2	108.4
$[Fe(CO)_4]^{2-}Li^+$	118.5	73.8	20.6	103.4
$[Fe(CO)_4]^{2-}Na^+$	119.5	73.9	20.7	99.4
$[Fe(CO)_4]^{2-}K^+$	120.4	78.8	30.6	101.9
$[Fe(CO)_4]^{2-}Rb^+$	119.6	90.6	58.8	104.2
$[Fe(CO)_4]^{2-}Cs^+$	120.5	102.3	88.3	110.3
		$p_{MC}{}^1$	$p_{MC}{}^2$	
$[Zn(CCH)_4]^{2-}Li^+$	105.0	89.9	65.8	123.1
$[Zn(CCH)_4]^{2-}Na^+$	107.7	93.3	71.9	120.0
$[Zn(CCH)_4]^{2-}K^+$	109.2	94.1	70.6	117.3
$[Zn(CCH)_4]^{2-}Rb^+$	110.0	97.5	77.0	116.5
$[Zn(CCH)_4]^{2-}Cs^+$	112.5	100.8	81.5	115.7
$[Cd(CCH)_4]^{2-}Li^+$	108.2	88.5	68.2	127.1
$[Cd(CCH)_4]^{2-}Na^+$	112.4	92.1	72.9	123.5
$[Cd(CCH)_4]^{2-}K^+$	115.0	92.6	70.4	120.4
$[Cd(CCH)_4]^{2-}Rb^+$	114.8	95.7	75.8	119.4
$[Cd(CCH)_4]^{2-}Cs^+$	117.4	99.1	80.1	118.7
		p_{MO}	p_{MC}	
$[Zn(OCH_3)_4]^{2-}Li^+$	112.2	103.7	48.9	128.3
$[Zn(OCH_3)_4]^{2-}Na^+$	116.2	107.1	47.6	123.8
$[Zn(OCH_3)_4]^{2-}K^+$	119.7	110.8	41.5	120.8
$[Zn(OCH_3)_4]^{2-}Rb^+$	118.8	111.9	53.4	120.0
$[Zn(OCH_3)_4]^{2-}Cs^+$	120.0	116.4	65.5	120.1
		p_{MC}	p_{MH}	
$[Zn(CH_3)_4]^{2-}Li^+$	118.3	93.7	74.2	121.2
$[Zn(CH_3)_4]^{2-}Na^+$	121.1	94.7	79.5	115.5
$[Zn(CH_3)_4]^{2-}K^+$	121.4	101.9	75.2	115.6
$[Zn(CH_3)_4]^{2-}Rb^+$	121.3	104.4	83.9	114.4
$[Zn(CH_3)_4]^{2-}Cs^+$	125.4	108.2	87.4	112.8
		p_{MCl}		
$[ZnCl_4]^{2-}Li^+$	101.4	99.4		123.5
$[ZnCl_4]^{2-}Na^+$	104.3	103.6		119.9
$[ZnCl_4]^{2-}K^+$	104.1	106.5		117.8
$[ZnCl_4]^{2-}Rb^+$	105.1	108.6		117.3
$[ZnCl_4]^{2-}Cs^+$	106.6	112.4		116.8

simultaneously with several atoms of the molecular fragment rather than with a single localized site, which results in a diminishment of $V_{XC}(M,A)$. In contrast, ligands featuring positively charged atoms bound to the metal center, such as –CO, favor more isolated electrostatic contacts with the alkali metal and an increase in the magnitude of $V_{XC}(M,A)$. These systems display higher ICI_{XC} values (> 0.25), consistent with a reduction or absence of collective interaction.

Although it may appear counterintuitive that an exchange–correlation–based index is governed by atomic charges, a remarkably strong linear relationship ($R^2 = 0.99$) is observed between the boron atomic charge and $V_{XC}(M,A)$ (A being boron) in the TMB–alkali metal ion pairs. Interestingly, the correlation between the boron charge and the corresponding Coulombic term $V_C(M,A)$ (A being boron) is noticeably weaker, with an R^2 value of 0.90, suggesting that the exchange–correlation component is more correlated to variations in the boron electronic environment than the purely electrostatic interaction. Such correlation is not observed for transition metal ion pairs. Instead, clear linear relationships are found between the charge of the alkali metal cation and $V_{XC}(M,A)$ for several systems, including $[Zn(CCH)_4]^{2-}$ ($R^2 = 0.98$), $[Cd(CCH)_4]^{2-}$ ($R^2 = 0.98$), $[Zn(OCH_3)_4]^{2-}$ ($R^2 = 0.93$), and $[ZnCl_4]^{2-}$ ($R^2 = 0.97$), $[Fe(CO)_4]^{2-}$ ($R^2 = 0.96$), $[Co(CO)_4]^-$ ($R^2 = 0.87$). The only exception is $[Zn(CH_3)_4]^{2-}$, which displays a much weaker correlation ($R^2 = 0.28$), suggesting that the nature of the alkyl ligand significantly modulates the relationship between charge distribution and exchange–correlation interaction in these complexes.

The degree of interpenetration between the atoms participating in the interaction is closely related to the IQA energy components. For all studied systems, an increase in the M–A penetration index (p_{MA}) correlates with a higher absolute value of the exchange–correlation energy ($|V_{XC}(M,A)|$), reflecting enhanced orbital overlap between the alkali metal and the interacting atom. However, as we have seen before, lower $V_{XC}(M,A)$ values are associated with smaller ICI_{XC} indices, indicating that although M and A atoms may become more interpenetrated, such overlap does not promote collective interactions. In fact, large M–A penetration values correspond to interactions that remain classical rather than cooperative in nature ($[Zn(CH_3)_4]^{2-}$ systems show p_{MA} values up to 125%).

The energetic consequences of this behavior differ between the TMB–alkali metal pairs and the transition-metal–alkali metal complexes. In TMB systems, increasing p_{MA} results in more positive $E_{int}(M,A)$ values, meaning that the interaction becomes increasingly repulsive as penetration grows. Conversely, in transition metal complexes, greater interpenetration between M and A leads to less positive (i.e., less repulsive) $E_{int}(M,A)$ values, suggesting partial stabilization. This contrasting behavior can be rationalized by considering the Coulombic component $V_C(M,A)$, which directly reflects the charge distribution of M and A within each complex. In TMB systems, both interacting atoms carry positive charges, that of boron being greater than 1.8, giving rise to strong electrostatic repulsion upon closer approach. In transition-metal complexes, however, the presence of a more delocalized and partially negative electronic environment around A mitigates

TABLE 5 | Relevant atomic charges and IQA parameters for $M[AX_4]$ (M = Li^+, Na^+, K^+, Rb^+, Cs^+; A = Fe Co, Zn, Cd; X = –CO, –CCH, $–OCH_3$, $–CH_3$, and –Cl) ion pairs calculated at the B3LYP-D3BJ/def2-TZVPP level of theory. All energies are given in kcal mol^{-1}.

Ion pair	q(M)	q(A)	$q(X_C)$	$q(X_O)$	V_{XC}(M,A)	V_{XC}(M,T)	V_C(M,A)	V_C(M,T)	E_{int}(M,A)	E_{int}(M,T)
$[Co(CO)_4]^-Li^+$	0.909	0.350	0.843	−1.203	−11.6	−21.8	22.4	−123.9	10.9	−145.7
$[Co(CO)_4]^-Na^+$	0.851	0.420	0.850	−1.211	−14.9	−30.6	33.9	−87.5	19.0	−118.1
$[Co(CO)_4]^-K^+$	0.913	0.461	0.847	−1.231	−9.6	−26.9	39.0	−85.5	29.4	−112.5
$[Co(CO)_4]^-Rb^+$	0.905	0.464	0.852	−1.233	−10.0	−30.6	38.0	−81.1	28.1	−111.7
$[Co(CO)_4]^-Cs^+$	0.909	0.470	0.854	−1.236	−9.5	−32.2	36.9	−79.7	27.4	−111.9
$[Fe(CO)_4]^{2-}Li^+$	0.867	0.445	0.639	−1.273	−13.6	−29.0	36.6	−208.0	23.0	−237.0
$[Fe(CO)_4]^{2-}Na^+$	0.582	0.521	0.692	−1.267	−24.0	−52.2	35.2	−105.9	11.2	−158.1
$[Fe(CO)_4]^{2-}K^+$	0.659	0.557	0.678	−1.280	−19.9	−48.0	40.5	−113.7	20.7	−161.7
$[Fe(CO)_4]^{2-}Rb^+$	0.693	0.565	0.675	−1.285	−19.7	−51.6	42.2	−118.8	22.6	−170.4
$[Fe(CO)_4]^{2-}Cs^+$	0.803	0.583	0.655	−1.298	−13.9	−54.9	48.5	−144.2	34.6	−199.1
			$q(X_C{}^1)$	$q(X_C{}^2)$						
$[Zn(CCH)_4]^{2-}Li^+$	0.888	1.092	−0.317	−0.511	−1.9	−31.4	135.2	−235.9	133.2	−267.3
$[Zn(CCH)_4]^{2-}Na^+$	0.872	1.101	−0.292	−0.523	−2.3	−39.8	118.4	−196.2	116.1	−236.0
$[Zn(CCH)_4]^{2-}K^+$	0.864	1.103	−0.284	−0.519	−2.7	−47.8	107.4	−171.6	104.7	−219.3
$[Zn(CCH)_4]^{2-}Rb^+$	0.841	1.084	−0.274	−0.519	−3.2	−55.3	101.3	−160.8	98.1	−216.1
$[Zn(CCH)_4]^{2-}Cs^+$	0.839	1.084	−0.276	−0.517	−3.2	−58.9	100.0	−158.0	95.8	−216.9
$[Cd(CCH)_4]^{2-}Li^+$	0.885	0.992	−0.281	−0.529	−2.0	−31.7	116.0	−235.3	114.0	−267.0
$[Cd(CCH)_4]^{2-}Na^+$	0.867	0.996	−0.264	−0.535	−2.6	−40.4	101.7	−194.5	99.1	−234.9
$[Cd(CCH)_4]^{2-}K^+$	0.860	0.998	−0.259	−0.529	−3.2	−48.3	93.3	−169.0	90.0	−217.2
$[Cd(CCH)_4]^{2-}Rb^+$	0.845	1.000	−0.257	−0.523	−3.7	−53.5	90.2	−160.1	86.6	−213.6
$[Cd(CCH)_4]^{2-}Cs^+$	0.840	0.993	−0.257	−0.519	−3.8	−57.8	86.7	−156.2	82.9	−213.9
			$q(X_C)$	$q(X_H)$						
$[Zn(CH_3)_4]^{2-}Li^+$	0.871	0.879	−0.384	−0.175	−5.0	−40.3	120.7	−249.5	115.8	−289.8
$[Zn(CH_3)_4]^{2-}Na^+$	0.866	0.897	−0.362	−0.186	−6.2	−46.0	105.9	−204.2	99.7	−250.2

(Continues)

TABLE 5 | (Continued)

			$q(X_C)$	$q(X_H)$						
$[Zn(CH_3)_4]^{2-}K^+$	0.855	0.898	−0.343	−0.144	−6.0	−58.1	93.9	−178.9	87.9	−237.0
$[Zn(CH_3)_4]^{2-}Rb^+$	0.811	0.877	−0.342	−0.139	−7.6	−69.9	87.8	−162.9	89.2	−232.8
$[Zn(CH_3)_4]^{2-}Cs^+$	0.790	0.876	−0.347	−0.136	−8.8	−76.8	85.8	−156.8	76.9	−233.6
			$q(X_O)$	$q(X_C)$						
$[Zn(OCH_3)_4]^{2-}Li^+$	0.890	1.314	−1.235	0.636	−1.2	−41.1	178.2	−274.4	177.0	−315.5
$[Zn(OCH_3)_4]^{2-}Na^+$	0.882	1.324	−1.225	0.650	−1.6	−47.7	157.4	−226.8	155.8	−274.5
$[Zn(OCH_3)_4]^{2-}K^+$	0.897	1.329	−1.218	0.651	−2.3	−56.9	144.7	−203.0	142.4	−256.0
$[Zn(OCH_3)_4]^{2-}Rb^+$	0.856	1.305	−1.202	0.638	−2.6	−65.8	137.6	−193.8	135.0	−259.6
$[Zn(OCH_3)_4]^{2-}Cs^+$	0.854	1.312	−1.201	0.636	−2.2	−70.4	137.4	−194.1	135.2	−264.5
			$q(X_{Cl})$							
$[ZnCl_4]^{2-}Li^+$	0.889	1.173	−0.788		−1.2	−31.7	140.7	−228.6	139.5	−260.2
$[ZnCl_4]^{2-}Na^+$	0.878	1.181	−0.783		−1.4	−38.8	125.1	−190.8	123.7	−229.6
$[ZnCl_4]^{2-}K^+$	0.871	1.187	−0.780		−1.5	−47.2	112.1	−169.5	110.6	−216.7
$[ZnCl_4]^{2-}Rb^+$	0.847	1.160	−0.766		−1.8	−55.3	104.3	−160.6	102.6	−215.9
$[ZnCl_4]^{2-}Cs^+$	0.848	1.162	−0.766		−1.7	−57.6	101.9	−157.2	100.3	−214.8

TABLE 6 | Coulombic (ICI_C) and exchange-correlation (ICI_{XC}) interaction collectivity index values for $M[AX_4]$ (M = Li^+, Na^+, K^+, Rb^+, Cs^+; A = Fe, Co, Zn, Cd; X = –CO, –CCH, $–OCH_3$, $–CH_3$, and –Cl) ion pairs calculated at the B3LYP-D3BJ/def2-TZVPP level of theory.

Ion pair	ICI_C	ICI_{XC}
$[Co(CO)_4]^-Li^+$	−0.181	0.529
$[Co(CO)_4]^-Na^+$	−0.387	0.486
$[Co(CO)_4]^-K^+$	−0.456	0.355
$[Co(CO)_4]^-Rb^+$	−0.469	0.325
$[Co(CO)_4]^-Cs^+$	−0.463	0.295
$[Fe(CO)_4]^{2-}Li^+$	−0.176	0.469
$[Fe(CO)_4]^{2-}Na^+$	−0.332	0.459
$[Fe(CO)_4]^{2-}K^+$	−0.357	0.414
$[Fe(CO)_4]^{2-}Rb^+$	−0.355	0.381
$[Fe(CO)_4]^{2-}Cs^+$	−0.337	0.253
$[Zn(CCH)_4]^{2-}Li^+$	−0.585	0.061
$[Zn(CCH)_4]^{2-}Na^+$	−0.603	0.056
$[Zn(CCH)_4]^{2-}K^+$	−0.626	0.056
$[Zn(CCH)_4]^{2-}Rb^+$	−0.630	0.057
$[Zn(CCH)_4]^{2-}Cs^+$	−0.627	0.055
$[Cd(CCH)_4]^{2-}Li^+$	−0.493	0.062
$[Cd(CCH)_4]^{2-}Na^+$	−0.523	0.064
$[Cd(CCH)_4]^{2-}K^+$	−0.552	0.067
$[Cd(CCH)_4]^{2-}Rb^+$	−0.563	0.068
$[Cd(CCH)_4]^{2-}Cs^+$	−0.555	0.066
$[Zn(CH_3)_4]^{2-}Li^+$	−0.484	0.123
$[Zn(CH_3)_4]^{2-}Na^+$	−0.518	0.134
$[Zn(CH_3)_4]^{2-}K^+$	−0.525	0.103
$[Zn(CH_3)_4]^{2-}Rb^+$	−0.539	0.108
$[Zn(CH_3)_4]^{2-}Cs^+$	−0.547	0.115
$[Zn(OCH_3)_4]^{2-}Li^+$	−0.649	0.028
$[Zn(OCH_3)_4]^{2-}Na^+$	−0.694	0.033
$[Zn(OCH_3)_4]^{2-}K^+$	−0.712	0.039
$[Zn(OCH_3)_4]^{2-}Rb^+$	−0.710	0.040
$[Zn(OCH_3)_4]^{2-}Cs^+$	−0.708	0.031
$[ZnCl_4]^{2-}Li^+$	−0.616	0.037
$[ZnCl_4]^{2-}Na^+$	−0.655	0.036
$[ZnCl_4]^{2-}K^+$	−0.661	0.033
$[ZnCl_4]^{2-}Rb^+$	−0.650	0.032
$[ZnCl_4]^{2-}Cs^+$	−0.649	0.029

this repulsion by diminishing the positive charge of the metal center, allowing increased M–A penetration to contribute slightly to stabilization.

As illustrated in Figure 1, the penetration index between atoms M and A (p_{MA}) exhibits strong linear correlations with all IQA energy components for the systems that display collective interactions. This clear linear behavior indicates a direct and coherent relationship between atomic interpenetration of the cation and the central atom in the anion and the energetic descriptors derived from the IQA analysis. In contrast, such correlations become significantly weaker, or even vanish entirely, for systems dominated by classical (noncollective) interactions. The complex $[Zn(CH_3)4]^{2-}$ represents an intermediate case, displaying moderate linear relationships (R^2 values between 0.3 and 0.75), consistent with its partially collective bonding character (see Table 6). These observations strongly suggest that the degree of collectivity in alkali metal cation–anionic complex interactions is intrinsically determined by the nature of the M–A interaction itself.

Some interesting trends are also found by analyzing the role of the tetrahedral angle α (Tables 1 and 4). For systems exhibiting collective interactions, the α angles systematically decrease with increasing alkali metal cation size. In contrast, carbonyl compounds, which display noncollective behavior, show the opposite trend, with α increasing down the alkali metal group. Interestingly, the α angle plays a key role in determining the magnitude of the exchange–correlation contribution within the IQA framework, V_{XC}(M,T). Smaller α angles lead to enhanced exchange–correlation stabilization.

Generally, larger α angles are associated with collective interactions. In transition metal complexes exhibiting collective character, α values range from 115° to 128°, whereas noncollective systems display smaller angles, typically between 99° and 110°. Notably, in TMB systems, α angles in the narrower range of 104°–109° are also indicative of collective interactions, highlighting a distinct geometric signature for this class of compounds.

4 | Conclusions

This study provides compelling evidence that collective interactions, originally identified in organometallic complexes, can also operate in ion pairs traditionally viewed as dominated by electrostatics. Our results for alkali metal–tetramethylborate and transition metal tetrahedral anions demonstrate that these interactions arise from the cooperative participation of multiple atoms in the stabilization of the cation–anion pair.

In all systems analyzed, the IQA decomposition reveals that the direct metal–central-atom (M···A) interaction is predominantly repulsive and weakly covalent, while the main stabilizing contribution originates from the interaction of the metal with the peripheral substituents (M···X). The low exchange–correlation interaction collectivity indices ($ICI_{XC} < 0.07$) observed for systems containing –CCH, $–OCH_3$, and –Cl ligands confirm the presence of highly collective interactions, where stabilization is distributed across several atoms rather than localized in a single pairwise bond. Conversely, systems with carbonyl ligands exhibit larger ICI_{XC} values (> 0.25), indicating a more conventional bonding pattern.

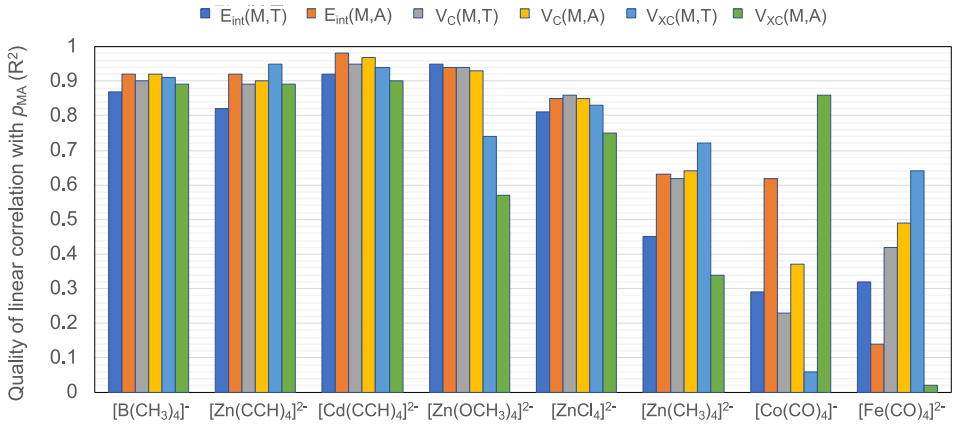

FIGURE 1 | Quality of the linear correlations (as R^2 value) between p_{MA} and different IQA energy parameters (E_{int}(M,T) in dark blue; E_{int}(M,A) in orange; V_C(M,T) in gray; V_C(M,A) in yellow; V_{XC}(M,T) in light blue; V_{XC}(M,A) in green) for all anions interacting with alkali metal cations (MAX_4 systems) studied in this work.

The observed trends reveal that the emergence of collective interactions depends on both geometry and electronic structure. Highly symmetrical or near-tetrahedral arrangements favor the simultaneous engagement of the cation with multiple electron-rich sites, while ligands with delocalized or polarized charge distributions enhance electronic collectivity. Altogether, these findings broaden the conceptual boundaries of chemical bonding by demonstrating that collective interactions are not restricted to covalent or multicenter systems but can also be significant in ionic species. Recognizing this collective character in common ion pairs might impact our understanding of ionic association, solvation, and reactivity in both molecular and solid-state chemistry.

Acknowledgments

This work was supported by projects PID2022-140244NB-I00 and PID2024-159030NA-I00 funded by MCIN/AEI/10.13039/501100011033 and by "ESF Investing in your future." Technical support from the Instituto de Biocomputación y Física de Sistemas Complejos (BIFI, Universidad de Zaragoza) is also acknowledged.

Funding

This work was supported by Ministerio de Ciencia e Innovación (PID2022-140244NB-I00, PID2024-159030NA-I00).

Data Availability Statement

The data that support the findings of this study are available from the corresponding author upon reasonable request.

References

1. G. Frenking, "Heretical Thoughts About the Present Understanding and Description of the Chemical Bond," *Molecular Physics* 121, no. 9–10 (2023): e2110168.

2. S. Sowlati-Hashjin, V. Šadek, S. Sadjadi, M. Karttunen, A. Martín-Pendás, and C. Foroutan-Nejad, "Collective Interactions Among Organometallics Are Exotic Bonds Hidden on Lab Shelves," *Nature Communications* 13, no. 1 (2022): 2069.

3. J. Poater, P. Vermeeren, T. A. Hamlin, F. M. Bickelhaupt, and M. Solà, "On the Existence of Collective Interactions Reinforcing the Metal-Ligand Bond in Organometallic Compounds," *Nature Communications* 14, no. 1 (2023): 3872.

4. V. Šadek, S. Sowlati-Hashjin, S. Sadjadi, M. Karttunen, A. Martín-Pendás, and C. Foroutan-Nejad, "Reply to: On the Existence of Collective Interactions Reinforcing the Metal-Ligand Bond in Organometallic Compounds," *Nature Communications* 14, no. 1 (2023): 3873.

5. P. Polestshuk, "An Approach to the Resolution of Dispute on Collective Atomic Interactions," *Nature Communications* 15, no. 1 (2024): 10404.

6. N. A. G. Bandeira, Á. Martín Pendás, and C. Foroutan-Nejad, "Reply to: An Approach to the Resolution of the Dispute on Collective Atomic Interactions," *Nature Communications* 15, no. 1 (2024): 10403, https://doi.org/10.1038/s41467-024-54553-y.

7. R. Pino-Rios, R. Báez-Grez, and C. Foroutan-Nejad, "Anti-Electrostatic Cation···π-Hole and Cation···Lp-Hole Interactions Are Stabilized via Collective Interactions," *Chemical Communications* 60, no. 4 (2024): 400–403, https://doi.org/10.1039/D3CC05451A.

8. P. L. A. Popelier, "Quantum Chemical Topology: On Bonds and Potentials," in *Intermolecular Forces and Clusters I*, ed. D. J. Wales (Springer Berlin Heidelberg, 2005), 1–56.

9. Z. Badri and C. Foroutan-Nejad, "Classical Versus Collective Interactions in Asymmetric Trigonal Bipyramidal Alkaline Metal–Boron Halide Complexes," *Chemistry—a European Journal* 30, no. 34 (2024): e202400156, https://doi.org/10.1002/chem.202400156.

10. D. M. Gil, J. Echeverría, and S. Alvarez, "Tetramethylammonium Cation: Directionality and Covalency in Its Interactions With Halide Ions," *Inorganic Chemistry* 61 (2022): 9082–9095, https://doi.org/10.1021/acs.inorgchem.2c00600.

11. J. Echeverría and S. Alvarez, "The Borderless World of Chemical Bonding Across the Van der Waals Crust and the Valence Region," *Chemical Science* 14, no. 42 (2023): 11647–11688, https://doi.org/10.1039/D3SC02238B.

12. B. Cordero, V. Gómez, A. E. Platero-Prats, et al., "Covalent radii revisited," *Dalton Transactions* 21 (2008): 2832–2838, https://doi.org/10.1039/B801115J.

13. S. Alvarez, "A Cartography of the Van der Waals Territories," *Dalton Transactions* 42, no. 24 (2013): 8617–8636, https://doi.org/10.1039/C3DT50599E.

14. J. Echeverría and S. Alvarez, "Widening the Scope of Structural Correlations by Means of the Van der Waals Crust Penetration Indices: The Dimerization of Groups 11 and 12 L–M–X Halo Complexes," *Crystal Growth and Design* 24, no. 11 (2024): 4743–4747, https://doi.org/10.1021/acs.cgd.4c00335.

15. J. D. Velasquez, N. Keshtkar, V. Polo, J. Munárriz, and J. Echeverría, "Unveiling the Potential of Haloalkenes as Electron Density Acceptors," *Crystal Growth and Design* 24, no. 13 (2024): 5775–5780, https://doi.org/10.1021/acs.cgd.4c00538.

16. A. M. Pendás, J. L. Casals-Sainz, and E. Francisco, "On Electrostatics, Covalency, and Chemical Dashes: Physical Interactions Versus Chemical Bonds," *Chemistry—a European Journal* 25, no. 1 (2019): 309–314, https://doi.org/10.1002/chem.201804160.

17. F. Wu, C. Deraedt, Y. Cornaton, et al., "Making Base-Assisted C–H Bond Activation by Cp*Co(III) Effective: A Noncovalent Interaction-Inclusive Theoretical Insight and Experimental Validation," *Organometallics* 39, no. 14 (2020): 2609–2629, https://doi.org/10.1021/acs.organomet.0c00253.

18. J. M. Guevara-Vela, K. Hess, T. Rocha-Rinza, Á. Martín Pendás, M. Flores-Álamo, and G. Moreno-Alcántar, "Stronger-Together: The Cooperativity of Aurophilic Interactions," *Chemical Communications* 58, no. 9 (2022): 1398–1401, https://doi.org/10.1039/D1CC05241A.

19. D. Barrena-Espés, V. Polo, J. Echeverría, Á. Martín Pendás, and J. Munárriz, "Metal–Ligand Cooperation in N–H Activation: Bridging Electron-Pushing Formalism and Energy Descriptors," *Inorganic Chemistry* 64, no. 43 (2025): 21452–21464, https://doi.org/10.1021/acs.inorgchem.5c03268.

20. A. Caballero-Muñoz, J. M. Guevara-Vela, A. Fernández-Alarcón, et al., "Structural Diversity and Argentophilic Interactions in Small Phosphine Silver(I) Thiolate Clusters," *European Journal of Inorganic Chemistry* 2021, no. 27 (2021): 2702–2711, https://doi.org/10.1002/ejic.202100336.

21. Á. Martín Pendás, E. Francisco, D. Suárez, et al., "Atoms in Molecules in Real Space: A Fertile Field for Chemical Bonding," *Physical Chemistry Chemical Physics* 25, no. 15 (2023): 10231–10262, https://doi.org/10.1039/D2CP05540F.

22. M. J. Frisch, G. W. Trucks, H. B. Schlegel, et al., "Gaussian 16," Revision C.01, Wallingford, CT (2016).

23. F. Neese, "Software Update: The ORCA Program System—Version 5.0," *WIREs Computational Molecular Science* 12, no. 5 (2022): e1606, https://doi.org/10.1002/wcms.1606.

24. T. A. Keith, "T. K. Gristmill Software, Overland Park KS," AIMAll (Version 11.05.16), 2011, http://aim.tkgristmill.com/.

Supporting Information

Additional supporting information can be found online in the Supporting Information section. **Table S1:** Cartesian coordinates of all compounds optimized in this work.